THE OXYGEN EVOLUTION ON $La_{0.5}Ba_{0.5}CoO_3$

PASSIVATION PROCESSES

A.G.C. KOBUSSEN *, H. WILLEMS and G.H.J. BROERS

Department of Inorganic Chemistry, State University of Utrecht, Croesestraat 77A, 3522 AD Utrecht (The Netherlands)

ABSTRACT

Earlier publications on the oxygen evolution of $La_{0.5}Ba_{0.5}CoO_3$ have left a number of observations involving passivation effects of the electrode unexplained. Therefore, the electrode surface used was studied by means of X-ray powder diffraction and electron microscopy (with diffraction and elemental analysis). It could be concluded that the surface had partly been changed into (hydrated) cobalt oxides. From this and earlier experiments it was concluded that the $La_{0.5}Ba_{0.5}CoO_3$ electrode is activated by a (possibly diffusion-controlled) oxidation, but a further anodization at high overpotentials leads to passivation with loss of activity for the oxygen evolution. The activity is regained by lowering the overpotential.

INTRODUCTION

The oxygen evolution on semiconductor $La_{0.5}Ba_{0.5}CoO_3$ electrodes has been the subject of a number of publications. The temperature dependence [1] and reaction order towards hydroxyl ion at constant overpotential [2] have been determined in order to investigate the reaction mechanism. In these experiments a noticeable hysteresis was found. Later the impedance response [3,4] and the overpotential decay behaviour [5] were studied with particular attention to the adsorption behaviour and occurrence of intermediates. The final conclusion of these studies was that the actual evolution mechanism can be described by

$$OH^- \rightleftharpoons OH_{ad} + e \tag{1}$$

$$OH_{ad} + OH^- \rightleftharpoons O_{ad}^- + H_2O \tag{2}$$

$$O_{ad}^- \rightleftharpoons O_{ad} + e \tag{3}$$

$$O_{ad}^- + 2\,MeOOH \rightleftharpoons 2\,MeO_2 + H_2O + e \tag{3a}$$

---

* Present address: Materials Research Dept., VEG-Gasinstituut n.v., P.O. Box 137, 7300 AC Apeldoorn, The Netherlands.

$$2\ MeO_2 + H_2O \rightleftharpoons 2\ MeOOH + O_{ad} \tag{3b}$$

$$O_{ad} + OH^- \rightarrow O_2H_{ad}^- \quad rds \tag{4}$$

$$O_2H_{ad}^- + OH^- \xrightarrow{fast} O_2 + H_2O + 2\ e \tag{5}$$

Here an alternative to step (3) has also been given so as to include successive stages of surface oxidation (steps 3a, b). These steps are modifications of the ones suggested by Krasil'shchikov [6] for oxygen evolution at nickel-based nickel oxide electrodes. The principal difference between this mechanism and that of Krasil'shchikov is that a fourth (rate-determining) step leading to perhydroxyl is substituted for the recombination of adsorbed oxygen atoms to molecules. This is the more likely pathway for small surface concentrations of adsorbed O (low θ_2), since then the recombination probability is low. Adsorbed OH, O and possibly O^- species are involved as intermediates in the reaction. By assuming the second (chemical) quasi-equilibrium to lie far to the left in the entire overpotential region, the surface concentration of O^- becomes extremely low so that steps (2) and (3), or alternatively (2) and (3a), effectively merge into a single (quasi-equilibrium) step. From our previously reported experiments [4,5], it was concluded that the O atom adsorption involves low fractional surface coverages only, but the adsorption of, for example, OH radicals leading to a broad pseudo-capacitance maximum points to appreciable Frumkin-type interactions.

However, a number of observations from earlier experiments are left unexplained by this mechanism, and these are summarized below.

(1) Severe hysteresis in the current density occurred for a slow potentiostatic sweep [1,2], see Figure 1. The current density deviates from the theoretically expected Tafel behaviour (at 60 mV/decade) above approx. 250 mV, and regains this behaviour again on returning below 250 mV. A decay in current is noticed on holding the (iR-free) overpotential at high values (> 300 mV). This typical current decay behaviour is also confirmed by the fact that the amount of hysteresis increases for slower sweep rates. If the hysteresis effect were caused by slow establishment of equilibrium the opposite should be expected.

(2) An additional admittance was found on a fresh electrode as compared to the simple RC parallel admittance proposed for an aged electrode [3]. This parasitical process is characterized by a fractional power frequency dependence. Within the measurement accuracy it can be represented by a semi-infinite diffusion impedance (Warburg) in series with a resistor. For the product $cD^{1/2}$ a value of 5×10^{-9} mol cm^{-2} s$^{-1/2}$ was found (where c and D are the concentration and diffusion coefficient respectively of the diffusing species).

(3) From the ageing behaviour of a fresh electrode an additional dc current (not leading to oxygen evolution) has been deduced. This current decreases in time, while simultaneously the main oxygen evolution current increases due to an increase in surface roughness (see Fig. 2).

(4) In earlier overpotential decay experiments [5] substantially slower decay rates were found for decays starting at stabilized overpotentials > 250 mV, if compared to those starting at lower overpotentials.
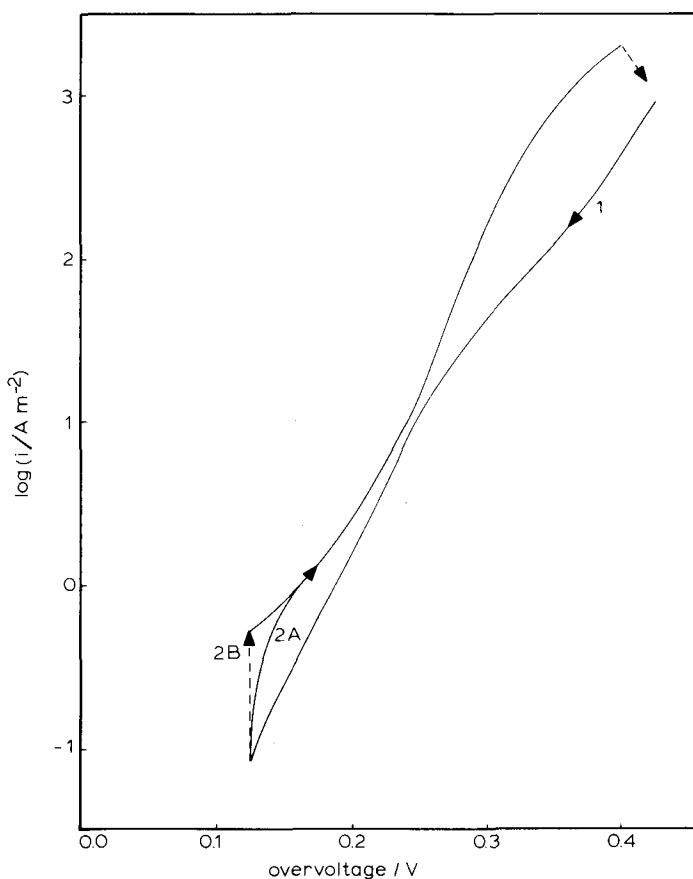
Fig. 1. From ref. 2. Current density during a slow voltage sweep on $La_{0.5}Ba_{0.5}CoO_3$ in $3\ M$ KOH solution (iR-corrected). Sweep-rate 0.1 mV s^{-1}. (1) Decreasing sweep after stabilizing at high potential; (2A) continuing increasing sweep without halt at low potential; (2B) increasing sweep after halt at low potential.

These observations all point to an additional "parasitical" process which might be the partial oxidation of the electrode material, as proposed by Matsumoto et al. [7] for (La, Sr)CoO$_3$ electrodes. However, by emission spectrography [8] and colorimetric analysis [2] of the used electrolyte, no dissolved constituent elements of the electrode material could be detected in our case, although after polarization black particles (probably eroded) were found on the electrode surface and in the electrolyte. The probably partial oxidation of $La_{0.5}Ba_{0.5}CoO_3$ at high overpotentials and the resulting decay in current density depreciate the otherwise favourable characteristics for oxygen evolution (380 mV polarization at 10^3 A m^{-2}). Therefore, we decided to check the electrode surface by means of X-ray powder diffraction and electron microscopy with elemental analysis for changes induced during prolonged oxygen evolution.

Severe hysteresis and a change in Tafel slope were found for a number of metals, e.g. Pt [9] and Ni [10–12]. For the behaviour of the latter electrode an acceptable explanation was given by Srinivasan and Lu [13]. On the basis of electrochemical
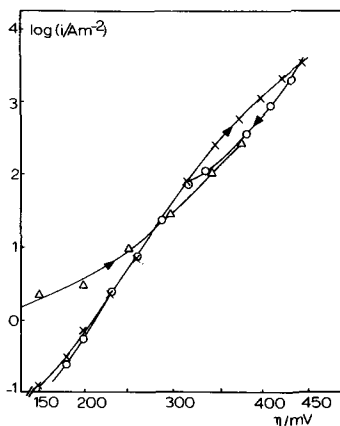

Fig. 2. From ref. 3. Logarithmic current density response as a function of overpotential for aged ($\times$, $\bigcirc$) and fresh ($\triangle$) $La_{0.5}Ba_{0.5}CoO_3$ electrodes in $6\,M$ KOH (sweep rate 2 mV min^{-1}, overpotentials iR-corrected).

and ellipsometric measurements they concluded on the existence of surface Ni-oxide layers which control the electrocatalytic activity of the electrode. The mechanism will then proceed as outlined above with Me = Ni, but now with step (3a) rate determining, leading to the Tafel slope of 40 mV/decade found experimentally. If instead of step (3a) an alternative oxidation of Ni^{III} takes place creating inactive Ni^{IV}-sites, gradually all surface oxides are trapped in this higher oxidation state, thereby decreasing the number of available Ni^{III}-sites. By subjecting the electrode to a relatively low overpoytential the electrode is "rejuvenated" in that inactive Ni^{IV}-sites are reduced to Ni^{III}-sites.

In view of the related nature of Co and Ni it was thought that this type of explanation would also apply to at least Co metal-based electrodes, but possibly also to $La_{0.5}Ba_{0.5}CoO_3$.

EXPERIMENTAL

Reflection powder diffraction photographs of the $La_{0.5}Ba_{0.5}CoO_3$ electrode surface were made by placing an electrode before and after a prolonged anodic polarization experiment in a Debye–Scherrer camera (Enraf-Nonius general-purpose camera, diam. 114.6 mm) by a Gandolphi attachment with goniometer head. This enabled the precise positioning of the electrode surface above the centre of the camera, and also the electrode could be oscillated to generate reflections over almost 360°.

Scanning electron microscopy (SEM) at 20 keV with qualitative analysis by means of a coupled Link Systems energy-dispersive analysis system was used to characterize electrode surfaces. Loose powder from the used (velvet-like) electrode surface was put on grids with ethanol and the observed in a transmission electron microscope (TEM) at 100 keV. From some particles electron diffraction patterns were recorded, which were standardized on the pattern of Au foil. Qualitative analysis was also performed on these particles in scanning mode (STEM) with the Link system.

RESULTS

Powder diffraction of $La_{0.5}Ba_{0.5}CoO_3$ electrodes

Preliminary powder diffraction patterns, obtained with a Guinier–Johansson camera on powder scraped off the surface of a used $La_{0.5}Ba_{0.5}CoO_3$ electrode, showed no extra lines when compared with a pattern of a fresh electrode. Therefore, Debye–Scherrer diffraction patterns of the intact surface layer before and after polarization were recorded. The polarized electrode was soaked in distilled water for 5 min to allow most of the KOH to diffuse out of the top surface layer. Then it was dried and fitted in the X-ray camera. Comparison of the diffraction pattern for a fresh and a polarized (approx. 2.5×10^5 C cm^{-2}) electrode revealed for the latter two faint extra lines which are given in Table 1.

TABLE 1

Extra X-ray powder diffraction lines of an aged electrode surface, and two electron diffraction patterns (TEM) of two seemingly amorphous particles. Also shown for comparison is the electron diffraction pattern of a used $NiCo_2O_4$ electrode, and a reference pattern of Ni_2O_3OH (the latter two patterns were reported by Trunov et al. [14])

X-ray powder diffraction of electrode surface $10d$/nm	TEM electron diffraction on two particles		Electron diffraction pattern of a used $NiCo_2O_4$ electrode $10d$/nm	Reference pattern of Ni_2O_3OH $10d$/nm
	$10d$/nm	$10d$/nm		
3.21	2.23	–	3.23	3.23
–	2.76	2.77	2.76	2.80
–	–	2.37	–	–
–	2.27	–	2.27	2.30
–	–	–	–	2.02
1.87	–	–	–	–
–	–	–	1.75	1.77
–	–	–	1.62	1.62
–	–	1.43	–	–

Electron microscopic examination of a $La_{0.5}Ba_{0.5}CoO_3$ electrode

After recording the powder diffraction pattern, one-half of the electrode surface was scraped off and set aside for examination by TEM. The remaining electrode was provided with a thin carbon film and observed by SEM. This (unscraped) surface layer was found to be all cracked and had partly flaked off. The flakes were approximately 4 μm thick. Elemental analysis (SEM) of the scraped surface, assumed to be essentially unchanged $La_{0.5}Ba_{0.5}CoO_3$, and the unscraped surface gave essentially the same composition. However, it is difficult to assess the effects of matrix absorption, so these results are not too reliable.

The scraped-off material consisted of very fine particles and was dispersed immediately on putting it in ethanol. Examination of grids loaded with these particles gave a range of particle diameters from 20 nm to 4 μm. However, the larger particles are conglomerates of smaller ones, and were mostly found to be amorphous. By electron diffraction in the TEM of two of these seemingly amorphous particles, faint diffraction spots could be obtained, from which the *d*-spacings shown in
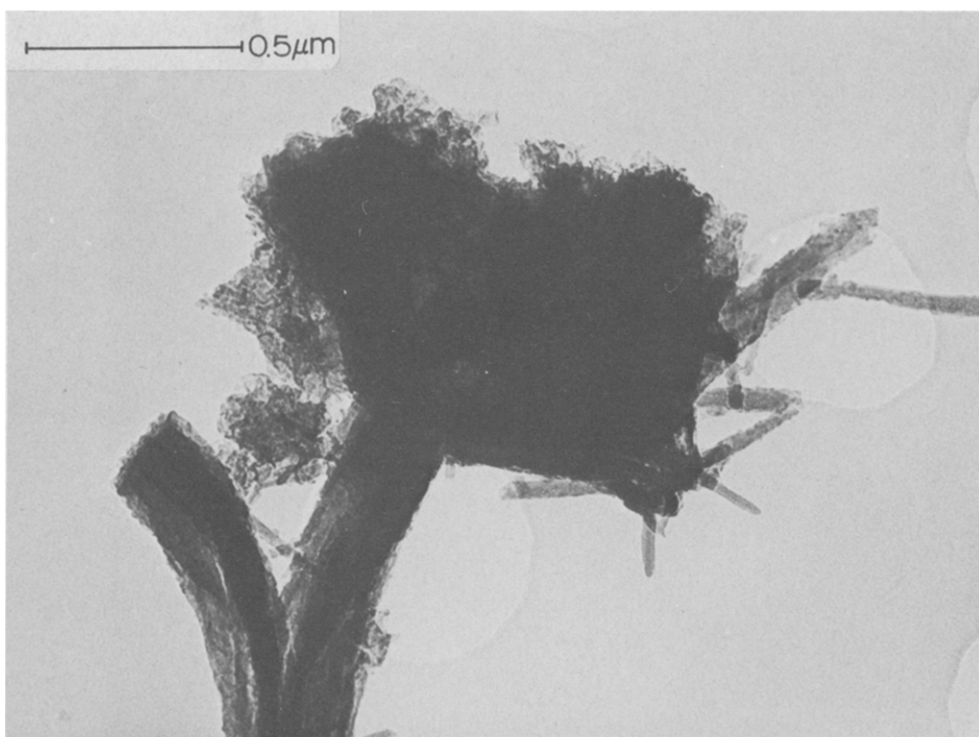

Fig. 3. TEM photo of some crystalline fibres found in the porous debris layer of a $La_{0.5}Ba_{0.5}CoO_3$ electrode after prolonged polarization.

TABLE 2

d-Spacings calculated from electron diffraction of a bundle of needle-like crystals (see Fig. 3)

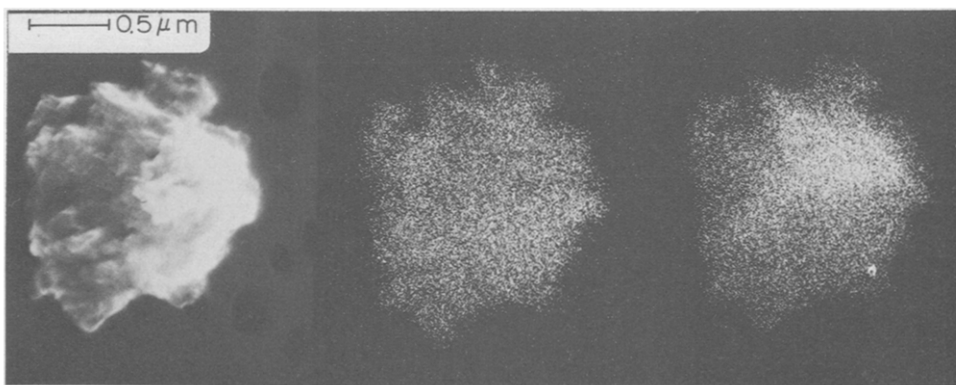| $10d/nm$		
5.8	1.95	1.46
5.45	1.88	1.31
3.28	1.86	1.27
2.50	1.84	1.24
2.29	1.69	

Fig. 4. STEM photo and mapping of Co signal (right) and of (La, Ba) signal (centre) of a seemingly amorphous particle from the porous debris layer of a $La_{0.5}Ba_{0.5}CoO_3$ electrode after prolonged polarization, showing inhomogeneous Co- and (La, Ba)-distributions.

Table 1 were calculated. Elemental analysis of the X-rays generated gave a composition of mostly Co and $< 10\%$ La and Ba.

Also prominent were needle-like crystals with a diameter of approximately 20 nm and lengths up to 0.8 μm (see Fig. 3). From a bundle of these crystals the electron diffraction pattern shown in Table 2 was obtained. Elemental analysis of these needle-like crystals gave a composition of mainly La and Co, in approximately equal quantities. Additional elemental analysis in the TEM of other amorphous particle conglomerates (diameter ≈ 1 μm) resulted in varying La : Co ratios (from 0.3 to 3).

In the scanning mode (STEM) the elemental composition of a conglomerate particle (diameter 1.3 μm) was recorded by mapping the Co and (La, Ba) signal, see Fig. 4. The latter signal could not be resolved into single elemental signals due to the partial overlap of the L-peaks of La and Ba. From the mapping the Co content was found to increase at the expense of the (La, Ba) content in the middle of the particle.

DISCUSSION

In Table 1 the diffraction patterns measured for the $La_{0.5}Ba_{0.5}CoO_3$ electrode surface and for some smorphous particles are compared to the diffraction pattern obtained by Trunov et al. [14] for the electrode surface of a $NiCo_2O_4$ electrode after polarization. As a reference, the d-spacings of Ni_2O_3OH are also given as reported in ref. 14. Analogous to the conclusions of Trunov et al., we suggest the transformation of the electrode surface into complex (hydrated) cobalt oxides. This also explains the high Co content in the amorphous-like particle conglomerates (Fig. 4) which are considered to originate from the transformed electrode surface.

On a fresh electrode the starting transformation seems to be diffusion controlled and characterized by the product $cD^{1/2} = 5 \times 10^{-9}$ mol cm^{-2} s$^{-1/2}$, which suggests an essentially homogeneous mass transport in the first stages of the process. Earlier, Takehara [15] found a diffusion-controlled oxidation of Ni-hydroxide in alkaline solutions, characterized by a value of $cD^{1/2} = 4 \times 10^{-8}$ mol cm^{-2} s$^{-1/2}$ for the diffusion of defects and protons. These species could similarly be involved in the present case, where the formation of the Co analogue of Ni_2O_3OH is presumed on the basis of the data in Table 1. Once this top layer of Co-oxides is formed it may take over the catalytic role in the oxygen evolution process of the original Co^{III}–Co^{IV} couple (present in the perovskite material). Analogous to the formation of inactive lattice-type Ni^{IV}-sites in Ni-oxides (discussed in the Introduction), further anodization of the newly formed Co-oxides can results in inactive Co^{IV}-sites. The Co^{IV} may be stabilized in the form of CoO_2-based layer-structured intercalation compounds where protons, K$^+$ and possibly Ba^{2+} ions can be incorporated to some (unknown) extent [16,17]. Lowering the potential causes decomposition of these compounds, thereby restoring the more favourable Co^{IV}/Co^{III} ratio for oxygen evolution.

The fact that no dissolved decomposition products are found in the electrolyte must mean that both the La and Ba constituents are retained in the active surface layer.

The stoichiometry and structure of the needle-like crystals, which consist predominantly of La and Co, is as yet not clear. Their occurrence can be explained in two ways. The crystals may either be formed in the process of oxygen evolution, for example by coprecipitation of La- and Co-hydroxides, or may already have been present as such in the bulk of the material. This latter hypothesis presupposes local inhomogeneities in the (La, Ba) distribution. Although from experiments it is known [18] that Ba is incorporated quantitatively in (La, Ba)CoO$_3$ at least up to the 50% level, Goodenough [19] also mentioned segregation of Sr for (La, Sr)CoO$_3$ resulting in Sr-rich and Sr-free areas, in order to explain results of magnetic measurements.

CONCLUSIONS

On the basis of the data presently available the passivation phenomena of the $La_{0.5}Ba_{0.5}CoO_3$ electrode in 6 M KOH at anodic overpotentials higher than about 250 mV cannot be resolved in detail. The following, however, can be concluded.

At least, parts of the eroded (porous) top surface layer of the electrode are not made up of $La_{0.5}Ba_{0.5}CoO_3$. Instead, the formation of hydrated Co-rich oxide multilayers still incorporating substantial amounts of La and/or Ba (hydr)oxides is proposed on the basis of the slow establishment of (at least quasi) steady states (10–20 h in decay experiments [5]) and the post-test analytical data presented above. The observed passivation and reactivation processes take place in the top layers of the electrode. The important role of "unstable" surface complexes [20] or "surface oxides" [10–12] in the oxygen evolution on $NiCo_2O_4$ and NiO_3 respectively is in agreement with the present findings. The question remains, however, whether the unchanged $La_{0.5}Ba_{0.5}CoO_3$ material is active towards the oxygen evolution reaction, or that the initial catalytic activity of these electrodes is also located in the transformed top layers. The major problem is that post-test analysis might not be truly representative for in situ conditions at the prevailing high potentials where Co^{IV} species in excess of that normally present (i.e. a Co^{IV}/Co^{III} ratio equal to unity in the bulk material) should be expected. For the present case, ellipsometry is not suitable to detect in situ changes at the very rough interface under varying high overpotentials.

It should finally be noted that the transformed oxide multilayer, although sensitive to passivation, effectively protects the perovskite substrate from further degradation over extended periods (several months).

ACKNOWLEDGEMENT

REFERENCES

1 A.G.C. Kobussen and H.J.A. van Wees in P. Vincenzini (Ed.), Energy and Ceramics, Proc. 4th Int. Meeting on Modern Ceramics Technologies, Saint-Vincent, Italy, May 1979, Elsevier, Amsterdam, p. 1019.
2 A.G.C. Kobussen and C.M.A.M. Mesters, J. Electroanal. Chem., 115 (1980) 131.
3 A.G.C. Kobussen, J. Electroanal. Chem., 126 (1981) 199.
4 A.G.C. Kobussen and G.H.J. Broers, J. Electroanal. Chem., 126 (1981) 221.
5 A.G.C. Kobussen, H. Willems and G.H.J. Broers, J. Electroanal. Chem., 142 (1982) 67.
6 A.N. Krasil'shchikov, Zh. Fiz. Khim., 37 (1963) 531.
7 Y. Matsumoto, H. Manabe and E. Sato, J. Electrochem. Soc., 127 (1980) 811.
8 A.G.C. Kobussen, F.R. van Buren, T.G.M. van den Belt and H.J.A. van Wees, J. Electroanal. Chem., 96 (1979) 123.
9 A. Damjanovic, A. Dey and J.O'M. Bockris, Electrochim. Acta, 11 (1966) 791.
10 B.E. Conway, M.A. Sattar and D. Gilroy, Electrochim. Acta, 14 (1969) 677.
11 M.A. Sattar and B.E. Conway, Electrochim. Acta, 14 (1969) 695.
12 B.E. Conway, M.A. Sattar and D. Gilroy, Electrochim. Acta, 14 (1969) 711.
13 P.W.T. Lu and S. Srinivasan in J.D.E. McIntyre, S. Srinivasan and F.G. Will (Eds.), Proc. Symp. Electrode Materials and Processes for Energy Conversion and Storage, Vol. 77-6, The Electrochemical Society, Princeton, 1977, p. 396.

14 A.M. Trunov, A.I. Kotseruba, N.M. Yakovleva and V.E. Polishchuk, Sov. Electrochem., 14 (1978) 1008.
15 Z. Takehara, Electrochim. Acta, 16 (1971) 833.
16 C. Delmas, C. Fouassier and P. Hagenmuller, J. Solid State Chem., 13 (1975) 165.
17 J.M. Gras and M. Pernot in J.D.E. McIntyre, S. Srinivasan and F.G. Wills (Eds.), Proc. Symp. Electrode Materials and Processes for Energy conversion and Storage, Vol. 77-6, The Electrochemical Society, Princeton, 1977, p. 425.
18 A.G.C. Kobussen, Thesis, Utrecht, 1981, Ch. 2.
19 J.B. Goodenough in H. Reiss (Ed.), Vol. 5, Progress in Solid State Chemistry, Pergamon, Oxford, 1971, p. 340.
20 D.B. Hibbert, J. Chem. Soc. Chem. Commun., (1980) 202.